Palestine Journal of Mathematics

Vol. 10(Special Issue I)(2021) , 83–92

STUDY OF MHD STEADY AND DYNAMIC CHARACTERISTICS OF PIVOTED CURVED SLIDER BEARING WITH A COUPLESTRESS FLUID

Hanumagowda B N, Salma A, Thippeswamy Gonchigara and Srikumar K

Communicated by Serkan Araci

MSC 2010 Classifications: Primary 76W99, 76D08, 76A05; Secondary 376D08,74DXX,76E25.

Keywords and phrases: MHD, Couple stress fluid, pivoted curved slider bearing.

Abstract Based on MHD thin film lubrication theory, the steady and dynamic attributes of pivoted curved slider bearings lubricated by couple stress fluid in the existence of a transverse magnetic field is theoretically studied. Considering the transient squeezing motion, the MHD dynamic Reynolds-type equation is derived from the continuity equation and the MHD motion equations. Expressions for the steady film pressure, load-carrying capacity, dynamic stiffness and damping coefficients are found and result are presented graphically. From the outcomes, it is observed that, the effect of magnetic fields signifies an enhancement in the film pressure. Overall, the applied magnetic-field effects characterized by the Hartmann number provide a significant increase in values of the load-carrying capacity, the stiffness coefficient and the damping coefficient as compared to the non-magnetic case. Also, the steady and dynamic features of the bearings enhance due to effect of couple stress fluid as compared with Newtonian case.

1 Introduction

Slider bearings are used to support the axial load in engineering disciplines. Analysis of the steady and dynamic characteristics of bearings is significant when studying the geometry of the bearing. The steady characteristics serve as a foundation for bearing construction, allowing for the avoidance of runner-pad interaction and the prediction of bearing stability, a study of dynamic characteristic shows more importance. Since slider bearing surfaces primarily work on the wedge action theory, considering the knowledge of dynamic stiffness and damping behaviour aids in bearing design. The liquid metals are excellent electrical conductors, and the load carrying capacity can be increased with the application of electromagnetic force. The impact of MHD on various bearing is carried out such as step slider bearing by Huges [1], Kuzma [2] studied MHD journal , Shukla [3] analyzed composite slider bearing, inertia effect for inclined bearing by Agarwal [4], and shown that the load enhances due to increase in magnetic field. Later, MHD lubrication of finite slider bearings is represent by Lin [5] and Lin et.al [6] revealed the dynamic properties of magnetic field plane slider bearing and found that the damping and stiffness coefficients are increasing. From past decades, the study of lubrication with non-Newtonian fluids has drawn attention of many investigators. Stokes [7] microcontinuum theory is the simplest generalization of classical fluid theory that allows for polar effects such as couple stresses and body couples. Numerous researchers have used couple stresses theory to explore the performance of distinctive bearings such as slider bearing by Ramanaiah and Sarkar [8] presented the squeeze film behavior of slider bearings, composite inclined step bearing by Sinha and Singh [9], Gupta. et. al [10] studied hydrostatic thrust bearings, Lin [11] analysed finite journal bearings and wide parabolic-shaped slider by Lin and Lu [12]. All these authors concluded that the effect of couple stress fluid enhances the load carrying capacity and reduces the friction coefficient as compared with Newtonian case. Several investigators are interested to study the combined effect of MHD and couple stress such as slider bearing by Das [13], Biradar and Hanumagowda [14] analysed composite slider bearing, sphere and plane surface by Naduvinamani.et.al [15], plane slider bearing by Hanumagowda [16] and Naduvinamani.et.al [17]–[18] studied static and dynamic characteristics of parabolic and plane inclined slider bearings and wide tapered land slider bearing. Based on their results obtained, it was concluded the effect of couple stress and MHD enhances the bearing characteristics as compared with non-magnetic and Newtonian case. Hanumagowda et al. [19]–[21] investigated the impact of couple stress and MHD on steady and dynamic features for various slider bearing and found that there is an improvement in steady and dynamic features Also, has extended his research to analyse Land-tapered slider bearing and porous exponential slider bearings. Hence, an endeavour has been made to examine the impact of MHD and CSF for pivoted curved slider bearing and to analysis steady and dynamic features.

2 Theoretical Analysis and Solution

The geometry of pivoted curved surface bearing lubricated with electrically couplestress fluid is presented in figure.1. Considering that the portion of curved surface is parabola,H_c is the height of the crown segment, h_1 and h_0 be the inlet and outlet film thickness, lower plate taken along x-axis, while lubricant film taken along y-axis. U be the velocity of moving curved surface and L be the length of pad in moving direction.

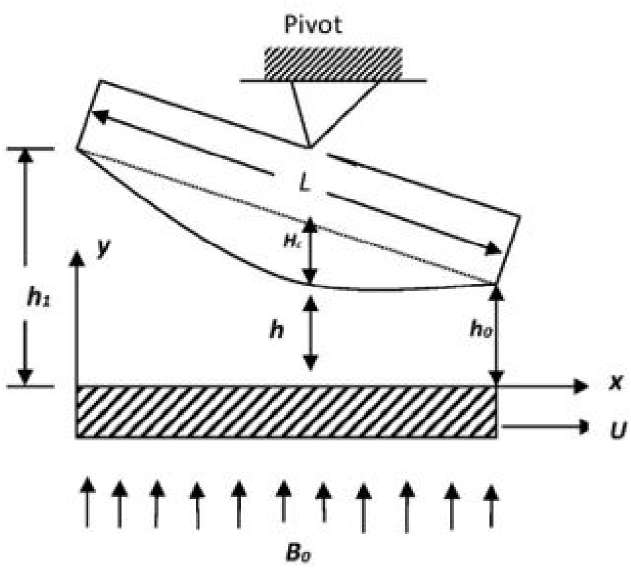

Figure 1. Geometry of pivoted curved slider bearing

Based on the standard assumptions, the relevant governing equations are:

$$\frac{\partial u}{\partial x} + \frac{\partial v}{\partial y} = 0 \tag{2.1}$$

$$\mu \frac{\partial^2 u}{\partial y^2} - \eta \frac{\partial^4 u}{\partial y^4} - \sigma B_0^2 u = \frac{\partial p}{\partial x} + \sigma E_z B_0 \tag{2.2}$$

$$\frac{\partial p}{\partial y} = 0 \tag{2.3}$$

$$\int\limits_{y=0}^{h} (E_z + B_0 u) dy = 0 \tag{2.4}$$

The fluid film thickness of pivoted curved slider bearing is

$$h = H_c \left\{ 4\left(\frac{x}{L} - \frac{1}{2}\right)^2 - 1 \right\} + h_0 \left\{ \frac{h_1}{h_0}\left(1 - \frac{x}{L}\right) + \frac{x}{L} \right\} \tag{2.5}$$

The velocity boundary conditions are:
At lower surface $y = 0$

$$u = \quad \frac{\partial^2 u}{\partial y^2} = 0 \quad v = 0 \tag{2.6}$$

At lower surface $y = h$

$$u = 0 \quad \frac{\partial^2 u}{\partial y^2} = 0 \quad v = \frac{dh}{dt} \tag{2.7}$$

The solution of Equation (2.1) by using the equation (2.4) with boundary conditions (2.6) and (2.7) is expressed as

$$u = -\frac{U}{2}T_1 - \frac{h_{m0}^2 h}{2l\mu M_0^2}\frac{\partial p}{\partial x}T_2 \tag{2.8}$$

Where

$$T_1 = T_{11} - T_{12}, T_2 = T_{13} - T_{14} \quad \text{for} \quad 4M_0^2 l^2/h_{m0}^2 < 1 \tag{2.9}$$

$$T_1 = T_{21} - T_{22}, T_2 = T_{23} - T_{24} \quad \text{for} \quad 4M_0^2 l^2/h_{m0}^2 = 1 \tag{2.10}$$

$$T_1 = T_{31} - T_{32}, T_2 = T_{33} - T_{34} \quad \text{for} \quad 4M_0^2 l^2/h_{m0}^2 > 1 \tag{2.11}$$

The associated equations for (2.9), (2.10) and (2.11) is discussed by Hanumagowda.et.al[19].
MHD Reynold's equation for pivoted curved slider bearing is

$$\frac{\partial}{\partial x}\left\{f(h,l,M_0)\frac{\partial p}{\partial x}\right\} = 6U\frac{\partial h}{\partial x} + 12\frac{\partial h}{\partial t} \tag{2.12}$$

Where,

$$f(h,l,M_0) = \begin{cases} \frac{6h_{m0}^2 h^2}{\mu l M_0^2}\left\{\frac{A^2 - B^2}{\frac{A^2}{B}\tanh\frac{Bh}{2l} - \frac{B^2}{A}\tanh\frac{Ah}{2l}} - \frac{2l}{h}\right\} & \text{for } 4M_0^2 l^2/h_{m0}^2 < 1 \\ \frac{6h_{m0}^2 h^2}{\mu l M_0^2}\left\{\frac{2\left(Cosh\left(h/\sqrt{2}l\right)+1\right)}{3\sqrt{2}sinh\left(h/\sqrt{2}l\right) - h/l} - \frac{2l}{h}\right\} & \text{for } 4M_0^2 l^2/h_{m0}^2 = 1 \\ \frac{6h_{m0}^2 h^2}{\mu l M_0^2}\left\{\frac{M_0(cosB_1 h + coshA_1 h)}{h_2(A_2 sinB_1 h + B_2 sinhA_1 h)} - \frac{2l}{h}\right\} & \text{for } 4M_0^2 l^2/h_{m0}^2 > 1 \end{cases}$$

$$A_2 = (B_1 - A_1 Cot\theta), \qquad B_2 = (A_1 + B_1 Cot\theta)$$

Following non-dimensional quantities is introduce in equation (2.12)

$$x^* = \frac{x}{L}, t^* = \frac{t}{h_{m0}}, P^* = \frac{p^* h_{m0}^2}{\mu U L}, l^* = \frac{2l}{h_{m0}}, M_0 = B_0 h_{m0}\left(\frac{\sigma}{\mu}\right)^{1/2}$$

$$h^* = h_1^* + (1 - h_1^* - 4\beta)\,x^* + 4\beta x^{*2}, h = H_c\left\{4\left(\frac{x}{L} - \frac{1}{2}\right)^2 - 1\right\} + \left\{\left(h_1 - h_1\frac{x}{L}\right) + h_0\frac{x}{L}\right\}$$

$$h^* = h_m^* + \{(\delta - 4\beta x^*)\,(1 - x^*)\}$$

The MHD Reynold's equation in non-dimensional form expressed as

$$\frac{\partial}{\partial x^*}\left\{f^*(h^*,l^*,M_0)\frac{\partial P^*}{\partial x^*}\right\} = 6\frac{dh^*}{dx^*} + 12V^* \tag{2.13}$$

where,

$$f^*(h^*,l^*,M_0)=\begin{cases}\frac{12h^{*2}}{l^*M_0^2}\left\{\frac{\left(A^{*2}-B^{*2}\right)}{\frac{A^{*2}}{B^*}\tanh\frac{B^*h^*}{l^*}-\frac{B^{*2}}{A^*}\tanh\frac{A^*h^*}{l^*}}-\frac{l^*}{h^*}\right\} & \text{for } M_0^2l^{*2}<1\\ \frac{12h^{*2}}{l^*M_0^2}\left\{\frac{1+cosh\left(\sqrt{2}h^*/l^*\right)}{\left(3/\sqrt{2}\right)sinh\left(\sqrt{2}h^*/l^*\right)-\left(h^*/l^*\right)}-\frac{l^*}{h^*}\right\} & \text{for } M_0^2l^{*2}=1\\ \frac{12h^{*2}}{l^*M_0^2}\left\{\frac{M_0(cosB_1^*h^*+coshA_1^*h^*)}{A_2^*sinB_1^*h^*+B_2^*sinhA_1^*h^*}-\frac{l^*}{h^*}\right\} & \text{for } M_0^2l^{*2}>1\end{cases}$$

$$A^*=\left\{\frac{1+\left(1-l^{*2}M_0^2\right)^{1/2}}{2}\right\}^{1/2},B^*=\left\{\frac{1-\left(1-l^{*2}M_0^2\right)^{1/2}}{2}\right\}^{1/2}$$

$$A_1^*=\sqrt{2M_0/l^*}\,Cos\left(\theta^*/2\right),B_1^*=\sqrt{2M_0/l^*}\,Sin\left(\theta^*/2\right),\theta^*=\tan^{-1}\left(\sqrt{l^{*2}M_0^2-1}\right)$$

$$A_2^*=\left(B_1^*-A_1^*Cot\theta^*\right),B_2^*=\left(A_1^*+B_1^*Cot\theta^*\right)$$

The equation for pressure is obtained by integrating equation (2.15) and using the boundary conditions of pressure and it is expressed as

$$P^*=6\int\limits_{x^*=0}^{x^*}\frac{h^*}{f^*(h^*,l^*,M_0)}dx^*+12V^*\int\limits_{x^*=0}^{x^*}\frac{x^*}{f^*(h^*,l^*,M_0)}dx^*+$$

$$\left\{-\frac{6\int\limits_{x^*=0}^{1}\frac{h^*}{f^*(h^*,l^*,M_0)}dx^*+12V^*\int\limits_{x^*=0}^{1}\frac{x^*}{f^*(h^*,l^*,M_0)}dx^*}{\int\limits_{x^*=0}^{1}\frac{1}{f^*(h^*,l^*,M_0)}dx^*}\right\}\int\limits_{x^*=0}^{x^*}\frac{1}{f^*(h^*,l^*,M_0)}dx^*\tag{2.14}$$

The load-carrying capacity expression is

$$w=\int\limits_0^L pdx$$

$$W^*=\int\limits_{x^*=0}^{1}p^*dx^*$$

The expression for the dimensionless load-carrying capacity is obtained, by taking into consideration the constant minimum film height and zero squeezing velocity

$$W^*=6\int\limits_0^1\int\limits_{x^*=0}^{x^*}\frac{h^*}{f^*(h^*,l^*,M_0)}dx^*dx^*+12V^*\int\limits_0^1\int\limits_{x^*=0}^{x^*}\frac{x^*}{f^*(h^*,l^*,M_0)}dx^*dx^*+$$

$$\left\{-\frac{6\int\limits_{x^*=0}^{1}\frac{h^*}{f^*(h^*,l^*,M_0)}dx^*+12V^*\int\limits_{x^*=0}^{1}\frac{x^*}{f^*(h^*,l^*,M_0)}dx^*}{\int\limits_{x^*=0}^{1}\frac{1}{f^*(h^*,l^*,M_0)}dx^*}\right\}\int\limits_0^1\int\limits_{x^*=0}^{x^*}\frac{1}{f^*(h^*,l^*,M_0)}dx^*dx^*\tag{2.15}$$

The expressions of steady film pressure P_s^* and steady load carrying capacity W_s^* in dimensionless form are

$$P_s^* = 6\int_{x^*=0}^{x^*} \frac{h^*}{f^*(h^*,l^*,M_0)}dx^* + \left\{ -\frac{6\int_{x^*=0}^{1} \frac{h^*}{f^*(h^*,l^*,M_0)}dx^*}{\int_{x^*=0}^{1} \frac{1}{f^*(h^*,l^*,M_0)}dx^*} \right\} \int_{x^*=0}^{x^*} \frac{1}{f^*(h^*,l^*,M_0)}dx^* \tag{2.16}$$

$$W_s^* = 6\int_{0}^{1}\int_{x^*=0}^{x^*} \frac{h^*}{f^*(h^*,l^*,M_0)}dx^*dx^* - \left\{ \frac{6\int_{x^*=0}^{1} \frac{h^*}{f^*(h^*,l^*,M_0)}dx^*}{\int_{x^*=0}^{1} \frac{1}{f^*(h^*,l^*,M_0)}dx^*} \right\} \int_{0}^{1}\int_{x^*=0}^{x^*} \frac{1}{f^*(h^*,l^*,M_0)}dx^*dx^* \tag{2.17}$$

The expressions for linear dynamic stiffness coefficient in dimensionless form is given by

$$S_d^* = -\left(\frac{\partial W_s^*}{\partial h_m^*}\right) \tag{2.18}$$

The expressions for linear dynamic damping coefficient in dimensionless form is given by

$$D_d^* = -\left(\frac{\partial W^*}{\partial V^*}\right) \tag{2.19}$$

3 Result and Discussion

The combined effect of magnetic field and CSF on the steady and dynamic features of pivoted curved slider bearing is analysed. The results so obtained are plotted graphically and discussed for various non-dimensional parameters such as M_0,l^*,δ ,h_m^*,β. The following range of values is considered to plot the graphs: $M_0 = 0-6, l^* = 0.0-0.6, \delta = 0.1-2.7, h_m^* = 0.8-1.4, \beta = 0.0-0.6$.

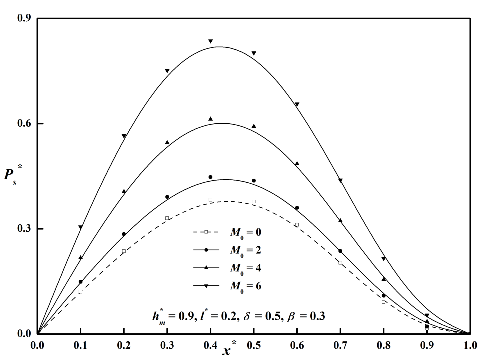

Figure-2: Variation of P_s^* along x^* for different values of M_0.

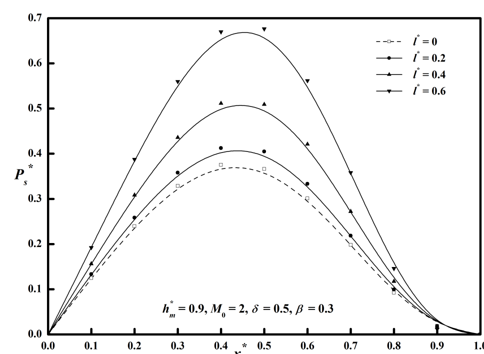

Figure-3: Variation of P_s^* along x^* for different values of l^*.

3.1 Dimensionless steady film pressure

The variation of dimensionless steady film pressure P_s^* as function M_0 is presented in Figure 2 against x^* and reported that the influence of the magnetic field $(M_0 = 2)$ is observed to increase the steady film pressure as compared to non-magnetic case. Increasing the values of Hartmann number$(M_0 = 4, 6, 8)$ enhances the steady film pressure. Figure 3 depicts the graph of P_s^* against x^* for distinctive l^* values and observed that, dotted line presents Newtonian case and solid lines for Non-Newtonian case and for increasing values of l^*, steady pressure P_s^* also enhances and reaches its maximum and decreases gradually. The deviation of P_s^* against x^* is displayed in Figure 4 for various values of h_m^* and found that steady pressure P_s^* decreases gradually for increasing h_m^* values. The profile of P_s^* as function of δ against x^* is elaborated in

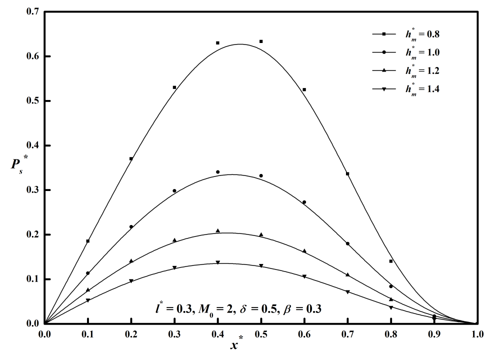

Figure-4: Variation of P_s^* along x^* for different values of h_m^*.

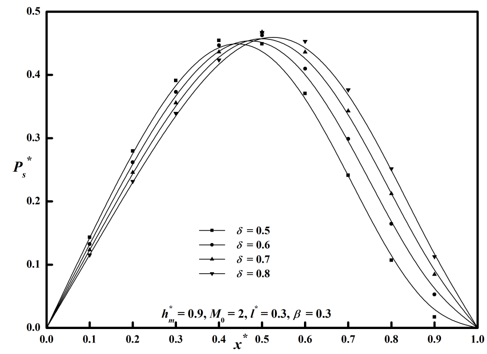

Figure-5: Variation of P_s^* along x^* for different values of δ.

Figure 5 and seen that due to increase in profile parameterδ, P_s^* decreases and reaches its maximum for certain value of x^* and later it increases. The graph of P_s^* against x^* for distinctive β values is depicted in Figure 6 and as result P_s^* increasing for increasing β values and attain maximum pressure but for some particular value of x^*, a reversed trend is observed.

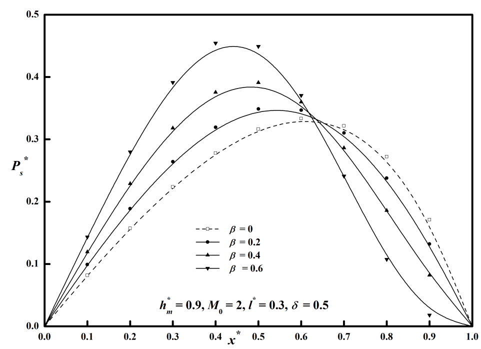

Figure-6: Variation of P_s^* along x^* for different values of β.

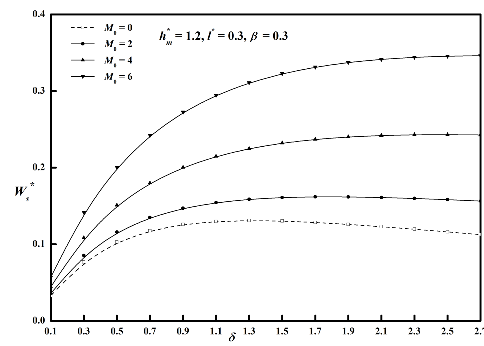

Figure-7: Variation of W_s^* along δ for different values of M_0.

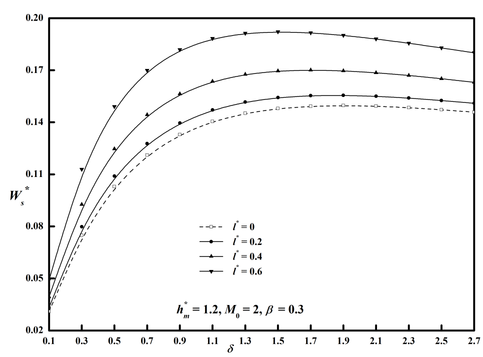

Figure-8: Variation of W_s^* along δ for different values of l^*.

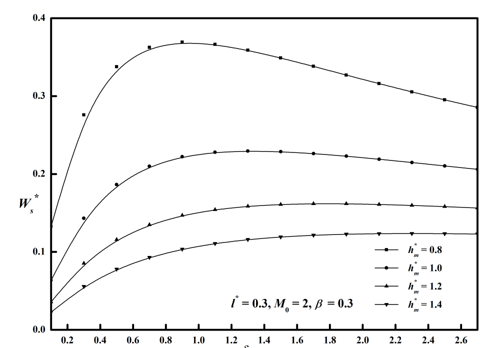

Figure-9: Variation of W_s^* along δ for different values of h_m^*.

3.2 Dimensionless Steady load carrying capacity

In Figure 7, the profile of dimensionless steady load carrying capacity W_s^* as function of Hartmann number M_0 against profile parameter δ is described. It is observed that the dotted line signifies non-magnetic case and solid lines signifies magnetic case and increase in W_s^* is found due to increase in M_0 values. In addition, larger increments are obtained with larger Hartmann numbers and larger profile parameters. The variation of W_s^* along δ for different l^* values is displayed in Figure 8 and found that steady load W_s^* is significant as compared to dotted line $(l^* = 0)$ for increasing values of l^*. In Figure 9, the graph of W_s^* as function of h_m^* is presented against δ values and observed that owing to increase in h_m^* values, load W_s^* decreases. The deviation of W_s^* against δ is illustrated in Figure 10 for distinct β values and noticed that the effect of β significantly increases the steady load.

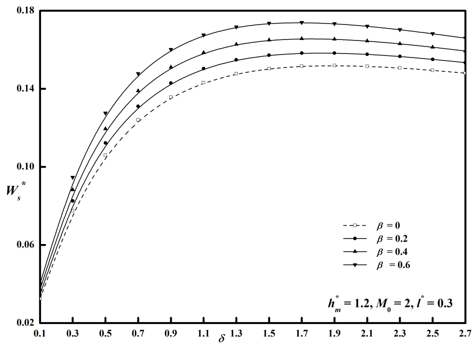

Figure-10: Variation of W_s^* along δ for different values of β .

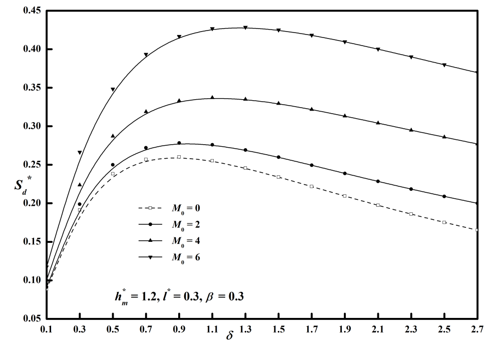

Figure-11: Variation of S_d^* along δ for different values of M_0 .

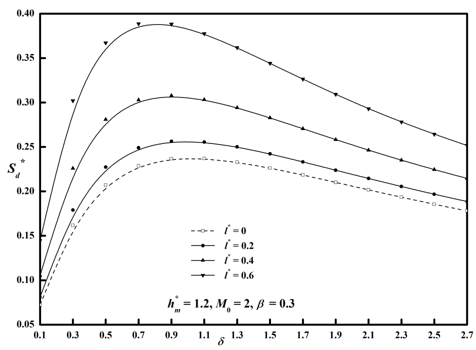

Figure-12: Variation of S_d^* along δ for different values of l^*.

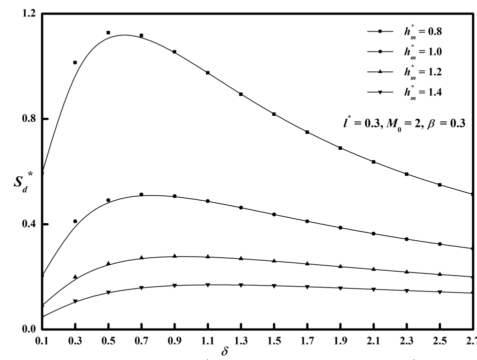

Figure-13: Variation of S_d^* along δ for different values of h_m^* .

3.3 Dynamic stiffness

Figure 11 depicts the deviation of dynamic stiffness S_d^* against profile parameter δ for different M_0 values and noticed that S_d^* raises with increasing M_0 values as compared to dotted line. The graph of S_d^* as function of l^* is elaborated in Figure 12 against δ and observed that as compared to Newtonian case, dynamic stiffness is substantial for larger l^* values. In Figure 13, the variation of S_d^* against δ for distinct values of h_m^* is presented and seen that for decreasing values of h_m^* , S_d^* increases. The profile of S_d^* versus δ for various β values is explained in Figure 14 and found that dynamic stiffness significantly increases for larger β values. Also progressively decreases along profile parameter δ in all the four figures is noticed.

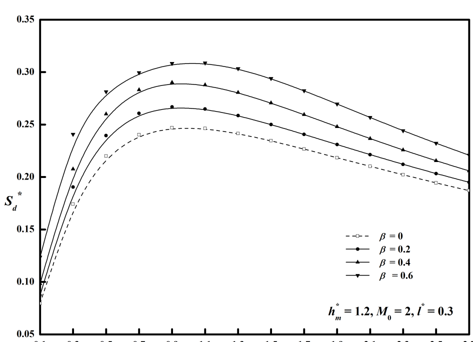

Figure-14: Variation of S_d^* along δ for different values of β.

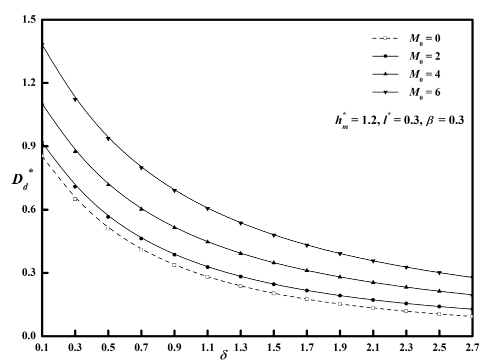

Figure-15: Variation of D_d^* along δ for different values of M_0.

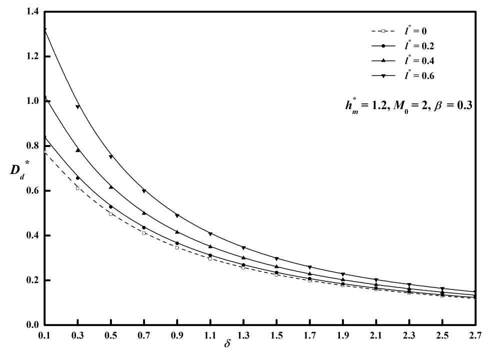

Figure-16: Variation of D_d^* along δ for different values of l^*.

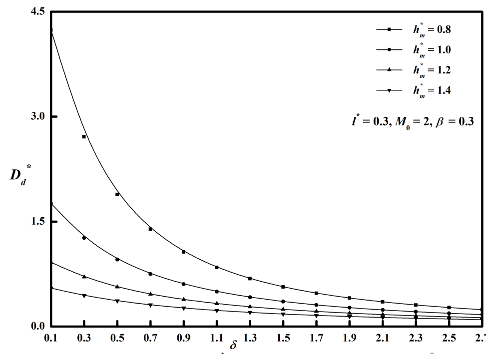

Figure-17: Variation of D_d^* along δ for different values of h_m^*.

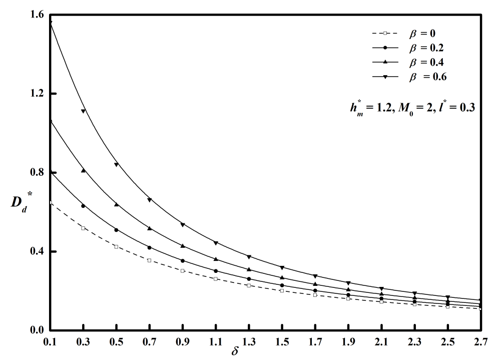

Figure-18: Variation of D_d^* along δ for different values of β.

3.4 Damping coefficient

The variation of damping coefficient D_d^* as function of Hartmann number against profile parameter δ is displayed in Figure 15. As result, the damping coefficient D_d^* increases as compared to dotted line $(M_0 = 0)$. In Figure 16, the deviation of D_d^* against δ is presented for various values l^* and observed that as compared to dotted line, damping coefficient enhances for larger values of l^*. Where as in Figure 17 presents the profile of D_d^* versus δ for various values of h_m^* and seen that D_d^* decreases due to increase in h_m^* values. The graph of D_d^* for different β values is explained in Figure 18 against profile parameter δ and found that damping coefficient is more pronounced for larger β values. Further from all four figures damping coefficient steadily decreases for increasing values of profile parameter δ.

4 Conclusion

The impact of MHD steady and dynamic characteristics of pivoted slider bearing lubricated with couple stress fluid is examined in the above section and the following conclusions are drawn from the outcomes obtained:

- An increase in steady pressure, steady load, damping coefficient and dynamic stiffness for larger values M_0 is noted compared to the Non-magnetic case.
- The steady and dynamic characteristic increases for increasing values of l^* in comparison with Newtonian case.
- It is also noticed that due to increase in minimum film height h_m^* the steady and dynamic features progressively decrease.
- For increasing β values, an enhancement is noticed in steady and dynamic features.
- The steady load, steady pressure, dynamic stiffness and damping coefficient decreases after attaining certain maximum value along profile parameter δ . The increasing values of δ results in decrease in the damping coefficient.

References

[1] W. F. Hughes, The Magnetohydrodynamic finite step slider bearing, *Journal of Basic Engineering*, **85**, 129–136 (1963).

[2] D.C Kuzma, The Magnetohydrodynamic journal bearing, *Journal of Basic Engineering*, **85(3)**, 424–427 (1963).

[3] J. B. Shukla., The Magnetohydrodynamic composite slider bearing, Wear, **7**, 460–465 (1964).

[4] V. K. Agarwal, Inertia effects in hydromagnetic inclined slider bearings*Japanese J.of Appl. Phy.*, **9(7)**,820–824 (1970).

[5] J.R. Lin, Magnetohydrodynamic lubrication of finite slider bearings, *Int. J. Appl. Mech. Eng.*, **7**, 1229–1246 (2002).

[6] J.R. Lin, C.R. Hung, C.H,Hsu., and C.Lai,Dynamic stiffness and damping characteristics of one-dimensional magneto-hydrodynamic inclined-plane slider bearings, *JET*, **223**, 211–219 (2009).

[7] V.K.Stokes, Couple stresses in fluids, *Physics of fluids*, **9**, 1709–1715 (1966).

[8] G.Ramanaiah and P.Sarkar, Slider bearings lubricated by fluids with couple stress, *Wear*, **52**, 27–36 (1979).

[9] P. Sinha and C. Singh, The effect of additives in the lubricant of a composite bearing with an inclined stepped surface, *Wear*, **66**, 17–26 (1981).

[10] R. S. Gupta. and L.G. Sharma., Analysis of couple stress lubricant in hydrostatic thrust bearings, *Wear*, **48**,257–269 (1988).

[11] Lin, Jaw-Ren., Effects of couple stresses on the lubrication of finite journal bearings, *Wear*,**206**, 171–178 (1997).

[12] J. R.Lin and Yu-Ming Lu., Steady-state performance of wide parabolic-shaped slider bearings with a couple stress fluid, *J. of Marine Sci. and Tech*, **12**, 239–246 (2004).

[13] N.C Das, A study of optimum load-bearing capacity for slider bearings lubricated with couple stress fluids in magnetic field, *Tribol. Int.*, **31**, 393-–400 (1998).

[14] K.Biradar and B.N. Hanumagowda, MHD effects on composite slider bearing lubricated with couple-stress fluids, *Tribology online*, **10**, pp 11–20 (2010).

[15] N.B Naduvinamani and M. Rajashekhar, MHD couple stress squeeze film characteristics between sphere and plane surface, *Tribol. Mater. Surf. Interfaces*, **5**, 94—99 (2011).

[16] B.N. Hanumagowda, Effect of magnetohydrodynamic and couple stress on steady and dynamic characteristics of plane slider bearing, *Tribology online*, **11(1)**, 40–49 (2016).

[17] N.B. Naduvinamani, A. Siddangouda and P. Siddharam, A comparative study of static and dynamic characteristics of parabolic and plane inclined slider bearings lubricated with MHD couple stress fluids, *Tribology Transactions*, **60**, 1–11 (2017).

[18] N. B. Naduvinamani, A. Siddangouda, Siddharama Patil and S Shridevi, Effect of couple stresses on static and dynamic characteristics of MHD wide tapered land slider bearing, *Sadhana*, **43**, 162–175 (2018).

[19] B. N. Hanumagowda., Thippeswamy Gonchigara., J. Santhosh Kumar and H. M.Shivakumar, Steady and dynamics characteristics of MHD Land- Tapered slider bearing: Use of Stoke-Couplestress Mode, *IJPAM*, **113**, 325-–333 (2017).

[20] B. N. Hanumagowda, Thippeswamy Gonchigara, J. Santhosh Kumar and H.M.ShivaKumar, Study of effect of magneto hydrodynamics and couple stress on steady and dynamic characteristics of porous exponential slider bearings, *JPCS*, **1000**, 1–12 (2018).

[21] B. N. Hanumagowda, Tesymol Cyriac, L. Kavitha and A Salma, Aanlysis of effect of magneto hydrodynamics and couple stress of steady and dynamic characteristics for porous secant slider bearings, *JPCS*, **1000**, 1–12 (2018).

Author information

Hanumagowda B N, Department of Mathematics, School of Applied Sciences, REVA University, Bangalore-560064, Karnataka, India.

Salma A, Department of Mathematics, School of Applied Sciences, REVA University, Bangalore-560064, Karnataka, India.

Thippeswamy Gonchigara, Department of Mathematics, GVPPGovt First Grade College, Bellary-583212, Karnataka, India.

Srikumar K, Department of Mathematics, Dayananda Sagar University, Bangalore-560068, Karnataka, India.
E-mail: hbn123@rediffmail.com

Received: Dec 20, 2020.
Accepted: Mar 12, 2021.